PNAS

Supporting Information for

Silver Electroceutical Technology to Treat Sarcopenia

Min Young Kim[a], Hyun Young Shin[b,c], Sung Chun Cho[d], Sohae Yang[a], Aseer Intisar[a], Hyeong Jung Woo[a], Youn-Seok Choi[e], Chang-Lim You[f], Jong-Sun Kang[f], Yun-Il Lee[d], Sang Chul Park[g], Kyungmoo Yea[a], Tae Gyu Oh[h], Michael Downes[h], Ronald M. Evans[h], Minseok S. Kim[a,b,i,j,*]

* Minseok S. Kim

Email: kms@dgist.ac.kr

This PDF file includes:

Supporting Text

Supplemental Results

Characterization of hYskMC and hAskMC. Prior to ES, we carried out characterization for the hYskMC and hAskMC. First, we analyzed the accumulation of lipofuscin and ROS levels, both of which tend to increase with cellular aging, using fluorescence-activated cell sorting (FACS) (SI Appendix, Fig. S5*A* and *C*) (1). The results showed an elevated level of lipofuscin and ROS in aged muscle cells (SI Appendix, Fig. S5*B* and *D*). Additionally, we compared the differentiation potential of hYskMC and hAskMC (SI Appendix, Fig. S6*A*-*F*) via the myotube formation and expression of genes related to proliferation (MyoD) and differentiation (MyoG, Myh1, and Mef2). Even without inducing differentiation, we observed a small amount of myotube formation in hYskMC. Moreover, while the expression of the proliferation marker decreased, the expression of genes related to differentiation increased substantially from the second and third days of differentiation. However, the myotube formation and the extent of upregulation in differentiation genes was significantly lower in hAskMC compared to the hYskMC, suggesting lower differentiation potential. Lastly, we compared the growth curve of hYskMC and hAskMC (SI Appendix, Fig. S6*G*), showing that the growth was slower in hAskMC compared to hYskMC. Thus, we verified that compared to the hYskMC, the hAskMC had increased lipofuscin accumulation, elevated ROS levels, reduced differentiation potential, and slower growth rate, which are characteristics of aged muscle cells. Since proliferation was significantly reduced beyond 6 passages, we used cells from passages 4 and 5 for the ES experiments.

Supplemental Methods

Simulation for optimizing the electric field uniformity of the HiTESS chip. The E-field simulation was performed using COMSOL 5.3a Multiphysics (COMSOL, Inc.) to secure a HiTESS platform with approximately 95% E-field uniformity. The E-field simulation was conducted using the electric current and electric circuit module in COMSOL. The electric potential, current density, total current, and uniformity varied according to the shape of the electrodes, such as the width, length, distance of the electrode, height of the culture medium, and pulse width (Fig. 2*E*). For the simulation, the geometry of the culture well, electrode, and culture medium were constructed via COMSOL built-in CAD (Computer-Aided Design), and the physical properties (medium conductivity 1.68 S/m, relative permittivity 80) of the simulation were entered (2). After the geometry and material setup, we set up the terminal electrode with a power supply circuit and ground to connect the electric circuit (*SI Appendix,* Fig. S2*B*). Using an electric circuit, we applied an electric pulse during the simulation. After setting up all the parameters, we computed the simulation using a time-dependent solver. For the analysis of results, the culture well surface was expressed in terms of the E-field (V/m) and electric current (mA) and quantified to calculate the average E-field and uniformity. Moreover, the electrode surface was expressed in terms of the electric current density (A/m2).

Construction of the HiTESS platform. The HiTESS platform comprised nine parts, including the control computer (Fig. 2*A* and *C*). The HiTESS substrate was fabricated by cleaning a 6-inch glass wafer (100 mm in diameter, 750 μm thick; Corning) via RCA cleaning and DI rinse. Electron beam (Sorona, SRN-200) evaporation of Ti/Au (20/200 nm) and photolithographic patterning were used to define the electrode shape. Subsequently, the wafer was coated with silicon oxide using plasma-enhanced chemical vapor deposition (KCT, KCT-800). Finally, the culture wells, electrode and electrode contact areas were etched on the surface coated with SiO2 through photolithography and a dielectric ICP etcher. The outer plastic and aluminum covers were designed using 3D computer-aided design (CAD) software (SolidWorks 2020, Dassault Systems), and all HiTESS parts were carved using a computer-numerical-control milling machine. The HiTESS pulse generator consisted of a microcontroller (PIC18(L)F2X/4XK22, Microchip Technology), digital-to-analog converter (TLV5624, Texas

Instruments), a complex programmable logic device (MAX II, AITERA), 10 ns switching multiplexers (AD8180, Analog Devices), octal sample-and-hold with multiplexed input (SMP08, Analog Devices), and feedback amplifier (LT1206, Linear Technology).

Analysis of Lipofuscin and ROS expression using Fluorescence-Activated Cell Sorting (FACS). We employed the FACS system (FACSAria III, BD) to investigate the differential expression of lipofuscin and ROS levels between young and aged skeletal muscle cells. We prepared a cell suspension of hAskMC and hYskMC in a FACS buffer (eBioscience™ Flow Cytometry Staining Buffer, Invitrogen). Lipofuscin is an autofluorescent material with excitation range of 360-480 nm, peaking at approximately 430 nm. Therefore, the FITC channel was utilized for lipofuscin detection. For ROS level assessment, cells were stained using 5 μM CELLROX™ Green (Invitrogen) and incubated for 30 minutes in complete culture media at 37°C, after which ROS was detected using the FITC channel as well. Before each cell sorting session, the FACSAria III system was calibrated according to the guidelines provided by the manufacturer. The cell suspension was loaded into the system and the fluorescence intensity was analyzed. Subsequent data analysis was performed using BD FACSDiva software.

Cultivation of human-derived primary skeletal muscle cell and electrical stimulation. Primary human skeletal muscle cells (SK-1111) from young males (aged 17 and 20 years) and aged males (aged 66 and 68 years) were purchased from Cook MyoSite. Each cell was grown in 25 T flasks in a growth medium (Myotonic basal medium (MB-2222, Cook Myosite) supplemented with 10% myotonic growth supplement (MB-3333, Cook Myosite) and 1% antibiotic-antimycotic solution (SV30079.01, HyCloneTM)). After two days of proliferation, the cells were subjected to a 3 min treatment with 0.05% trypsin-EDTA (Sigma). The cells were pelleted by centrifugation at 1200 rpm for 3 min and 1,200~1,300 cells were seeded per ES well. The method for precise cell seeding was the same as that described in a previous paper (3). Differentiation of cells was initiated on HiTESS substrate by changing the growth medium to a differentiation medium (MB-5555, Cook Myosite) supplemented with 1% antibiotic-antimycotic solution. Starting on day four of differentiation, ES screening was performed using the HiTESS platform for 2 h of stimulation of each culture well on the HiTESS substrate (*SI Appendix,* Fig. S7*A and B*). Specifically, the myotubes were continuously electrically stimulated at a frequency range of 0.1 to 5, 000 Hz with 0.01 ms pulse width.

Cryosection and immunostaining. The myotubes were fixed in 4% paraformaldehyde (R37814, Invitrogen) for 15 min and permeabilized with 0.5% Triton X-100 (Sigma). Subsequently, the myotubes were washed in PBS and incubated in a 2% BSA blocking solution. The samples were washed with 0.5% BSA and incubated with primary antibodies (MF-20, DSHB) for 2 h at RT. After washing three times with 0.5% BSA, the myotubes were incubated with the secondary antibody (Invitrogen) for 1 h at RT. Finally, the samples were washed five times in PBS and mounted with antifade mounting medium with DAPI (H-1200, VECTASHIELD®). Fluorescence images were obtained using a Nikon Ti2 full automated confocal microscope. NIS software was used for image acquisition, and the myotube diameter and number of nuclei/myotube were measured using IMARIS (Bitplane). The isolated TA muscle was embedded in the optimal cutting temperature (OCT) compound (Sakura Finetek). The sample was sectioned with a 7 μm-thick serial using a cryomicrotome (Tissue-Tek, Leica Microsystems). To measure the fiber size and Pax7 expression, we stained the samples in the following order: fixation, permeabilization, conjugation with laminin (Abcam), myosin heavy chain Type IIA (SC-71, DSHB), and Pax7 (Pax7, DSHB) for 2 h. Subsequently, the sections were washed in PBS three times for 3 min and incubated in the dark with secondary antibodies (Alexa Fluor 488 anti-mouse, Alexa Fluor 594 anti-rabbit, Invitrogen) for 1 h. We acquired the image with a Nikon Ti2 confocal microscope to evaluate the fiber cross-sectional area (CSA). The area of myofiber and Pax7 expression were measured using ImageJ software. The antibody lists are shown in *SI Appendix,* Table S2.

Senescence associated β-galactosidase (SA-β-Gal) assay. All staining experiments were conducted on the HiTESS substrate 24 h after ES application. SA-β-Gal staining was performed

according to the manufacturer's protocol using an SA-β-Gal kit (Cell Signaling Technology). SA-β-Gal increased in proportion to cell aging simultaneously with immunostaining. Images were acquired using an inverted microscope (Leica) for quantification, and the number of SA-β-Gal-positive myotubes was analyzed using IMARIS software.

Metabolic ability evaluation through MitoTracker™ Red FM staining. MitoTracker™ Red FM (ThermoFisher) intensity indicated the mitochondrial membrane potential. ATP production increases the mitochondrial membrane potential. After 24 hours of ES, for MitoTracker™ Red FM staining, myotubes in the HiTESS assembly were washed three times with DPBS. After washing, myotubes were incubated with MitoTracker™ Red FM stain buffer (differentiation medium with 250 nM MitoTracker™ Red FM) for 30 min and immediately imaged using a fully automated Nikon Ti2 A1R confocal microscope (Nikon). For the analysis, we used IMARIS for segmentation and intensity measurements. We imported the MitoTracker images into the IMARIS software. Subsequently, we employed the surface function to segment the regions expressing MitoTracker. Lastly, we measured the average intensity of the segmented regions to obtain quantitative results.

Calcium imaging. After 24 h of the application of the ES, the myotubes in the HiTESS assembly were loaded for 30 min with Fluo-8 calcium indicator dye from Fluo-8 Calcium Flux Assay Kit - No Wash (Abcam). Images were acquired using a Nikon Ti2 fully automated confocal microscope with a microscope cage incubator system HX (Live Cell Instrument) by applying each frequency of ES. The captured images were analyzed using ImageJ to count the total flash number, and SparkMaster, which is a plug-in for analyzing calcium spark intensity ($\Delta F/F0$) (4).

Real-time PCR. The myotubes were lysed in TRIzol (Thermo Fisher), and RNA isolation was performed using chloroform and isopropyl alcohol. Following reverse-transcription using TOPscript™ One-step RT PCR DryMIX (Enzynomics), cDNA synthesis was performed using Biometra T One 96G (Analytik Jena). Quantitative PCR was performed using KAPA SYBR FAST qPCR Master Mix (2X) (Kapa Biosystems) on a LightCycler® 480 (Roche) according to the manufacturer's instructions. The primer sequences are shown in *SI Appendix,* Table S3.

Simulation for in vivo electrical stimulation and ES intervention process. Before the in vivo experiment, a simulation was performed to apply the same conditions as in the in vitro experiment to optimize the electrodeposition and E-fields. For the simulation, the mouse muscle CT image was obtained using micro-CT (Quantum GX uCT, Perkin Elmer). The bones and muscles were reconstructed as a 3D mesh model using a built-in software. The 3D mouse model was imported to COMSOL Multiphysics, and the potential and location of the electrodes were optimized (Fig. 6*B*). The material properties used in the simulation are shown in *SI Appendix,* Table 4 (5). Female B57BL/6J mice (young mice of 4 months and aged mice of 24 months, Korea Research Institute of Bioscience and Biotechnology Laboratory Animal Resource Center) were used in this experiment. The animals were housed in a vivarium, with a regular 12 h day and night cycle, and water and food ad libitum. Mice were anesthetized with isoflurane (2% for initial, 0.5% for maintenance) vaporized using an isoflurane vaporizer (VIP 3000, MIDMARK). The maximum anesthetic time was limited to 40 min because of the rehabilitation function of the aged mice. Therefore, ES was applied to the mice for 30 min every day for six weeks. To attach the electrode, the fur on the legs was removed using a depilatory. To apply ES, the mice were fixed to a plastic plate, and electrodes connected to an 8-channel pulse generator were attached to each leg.

Isometric contractile force analysis. Electrically stimulated contractile force generation in the soleus muscle was measured using a force transducer (FT.03, Grass Instruments). The soleus

muscle was transferred to force the measurement devices. Both ends of the bundle were clipped at the measurement chambers containing Krebs-Ringer buffer and oxygenated with 95% O2 and 5% CO2 while being thermostatically maintained at 25°C. Tetanic contraction force was measured using an electrical stimulator (S48, Grass Instruments) under the stimulation conditions (Potential of 100 V, duration of 800 ms, frequency of 150 Hz). To determine the optimal muscle length, twitch contractions were induced by applying ES (1 Hz, 0.2 ms duration) and the muscle length was gradually increased to observe the maximum twitch force production.

Gene ontology analysis through RNA sequencing. Total RNA was extracted from tibialis anterior using TRIzol reagent, according to the manufacturer's instructions. RNA sequencing was performed by Ebiogen Corporation (Korea). The integrity and quality of the extracted RNA were confirmed using a 2100 Bioanalyzer (Agilent Technologies). The library was synthesized using the QuantSeq 3' mRNA Seq Library Prep kit for Illumina (Lexogen) according to the manufacturer's instructions. High-throughput sequencing was performed as paired-end sequencing using NovaSeq 6000 (Illumina). For data analysis, mRNA sequencing results were mapped using Bowtie2 to the reference genome. Read count calculations were processed using Bedtools based on unique and multiple alignments. The mapped mRNA sequencing results were quantile-normalized using EdgeR software. Normalized RNA-sequencing results were analyzed and visualized using ExDEGA Graphic Plus v2.0 (Ebiogen). The enrichment map was exported using CYTOSCAPE (V3.8.1; https://cytoscape.org/index.html).

Western blotting. Proteins were isolated from young and aged mice tibialis anterior (TA) muscle tissues using RIPA Lysis Buffer (Thermo Scientific) as per manufacturer's instructions. The proteins separation was caried out using 8% SDS-PAGE, followed by transfer to a PVDF membrane (Bio-Rad). To minimize non-specific binding, we blocked the membranes with 2% bovine serum albumin (BSA) at room temperature for 1 h. The membranes were then incubated overnight at 4°C with primary antibodies against Myosin, Beta-actin, and Atrogin-1 (*SI Appendix,* Table S2). After washing to remove excess antibodies, the membranes were treated with horseradish peroxidase-conjugated secondary antibodies (Invitrogen). We visualized the secondary antibodies using ECL Western blotting detection reagent (GE Healthcare). The images were obtained using Azure Imaging Systems (Azure biosystems). The captured images were analyzed using ImageJ.

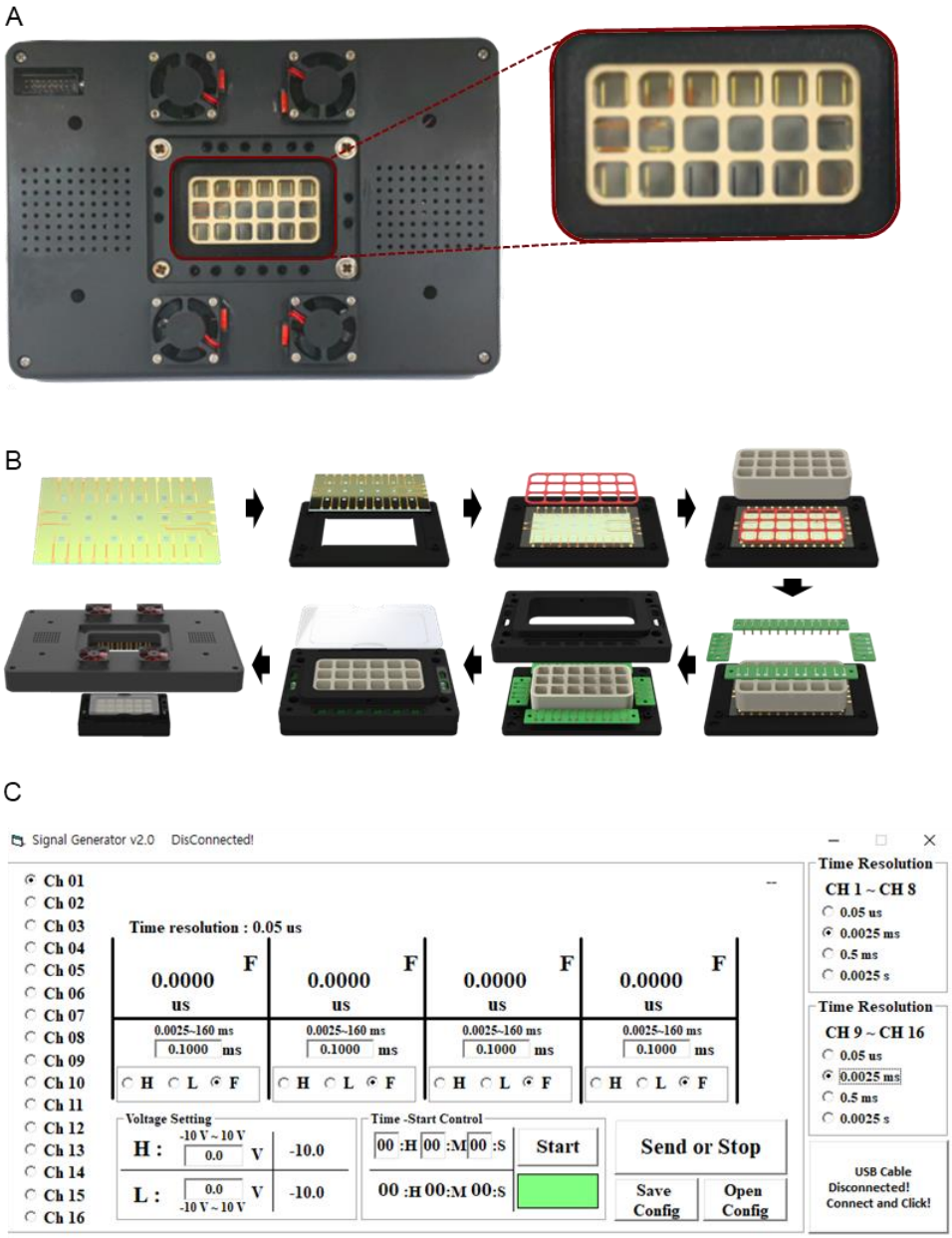

Fig. S1. Setup process of HiTESS platform. (A) HiTESS pulse generator integrated with the HiTESS device. (B) Assembly process of the HiTESS device. (C) Custom-made control software for simultaneous multiple ES.

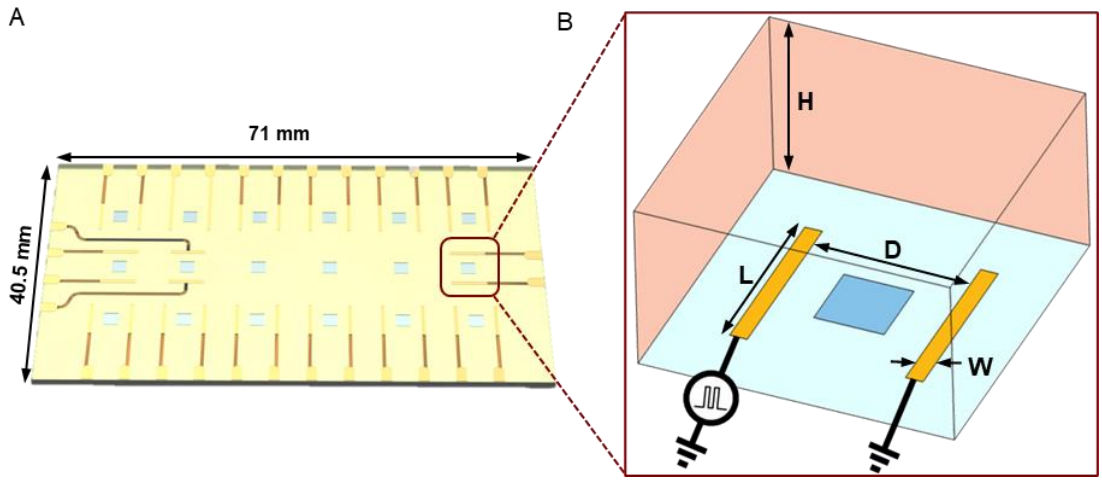

Fig. S2. Simulation parameters to optimize the HiTESS substrate. (A) Dimensions of the HiTESS substrate (B) Simulation parameters of the HiTESS substrate in a single chamber (H: height, L: length, D: distance, W: width) and circuit connection schematics.

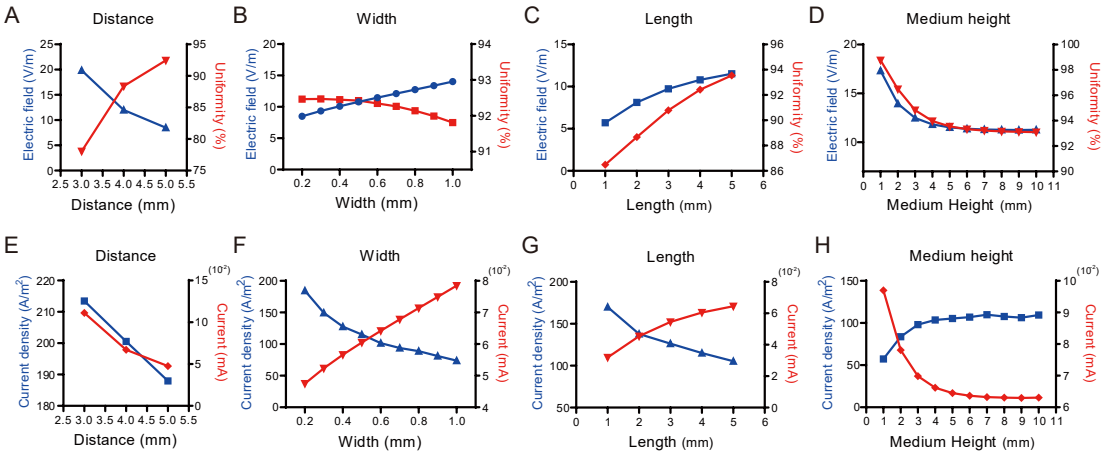

Fig. 3. Multiphysics simulation for electric field optimization (A-D) Simulation results of E-fields based on distance (A), width (B), length (C), and medium height (D). (E-H) Simulation results of current density on the electrodes and total current on culture well based on distance (E), width (F), length (G), and medium height (H).

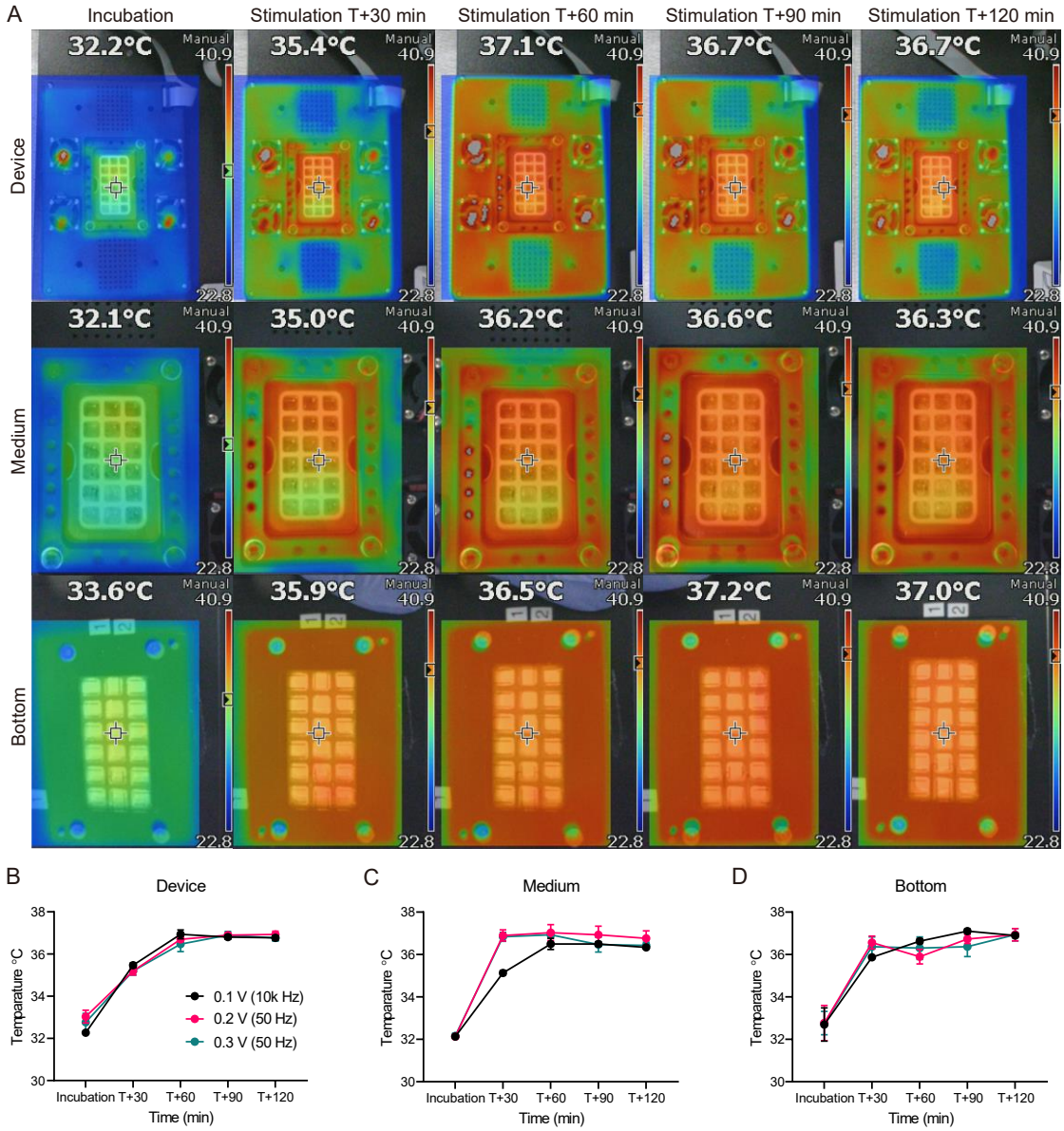

Fig. S4. Characterization of the heat generation in HiTESS platform. (A) Thermal images of the HiTESS device as position and operation time (B-D) Temperature change of device (B), medium (C), and bottom substrate (D) according to ES conditions. There was also no significant temperature change as time.

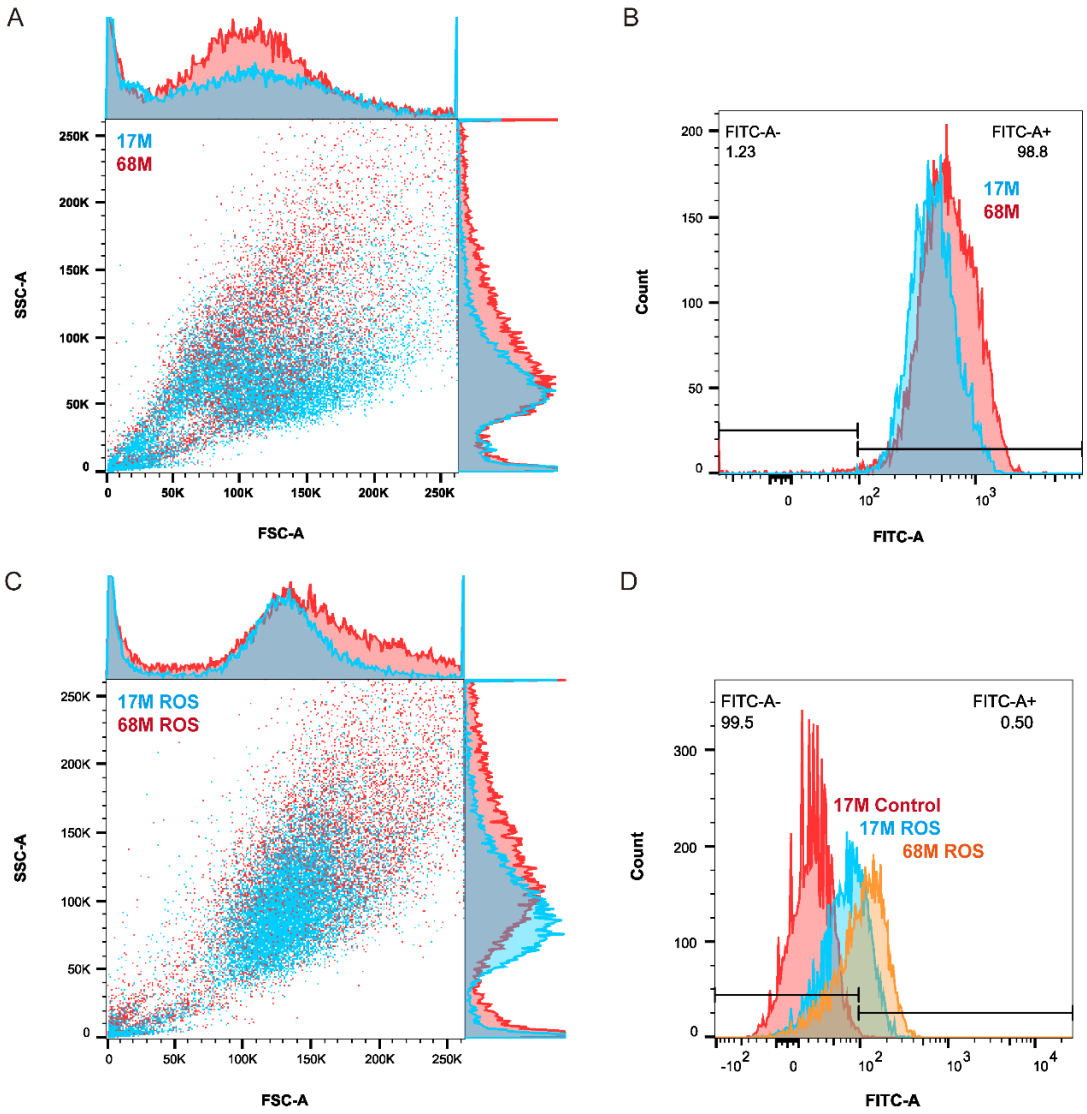

Fig. S5. Identification of lipofuscin and ROS using flow cytometry. (A and B) Difference in lipofuscin expression in hAskMC (68M) compared to hYskMC (17M) cells. (C and D) In hAskMC, intracellular ROS basal level is high compared with the hYskMC.

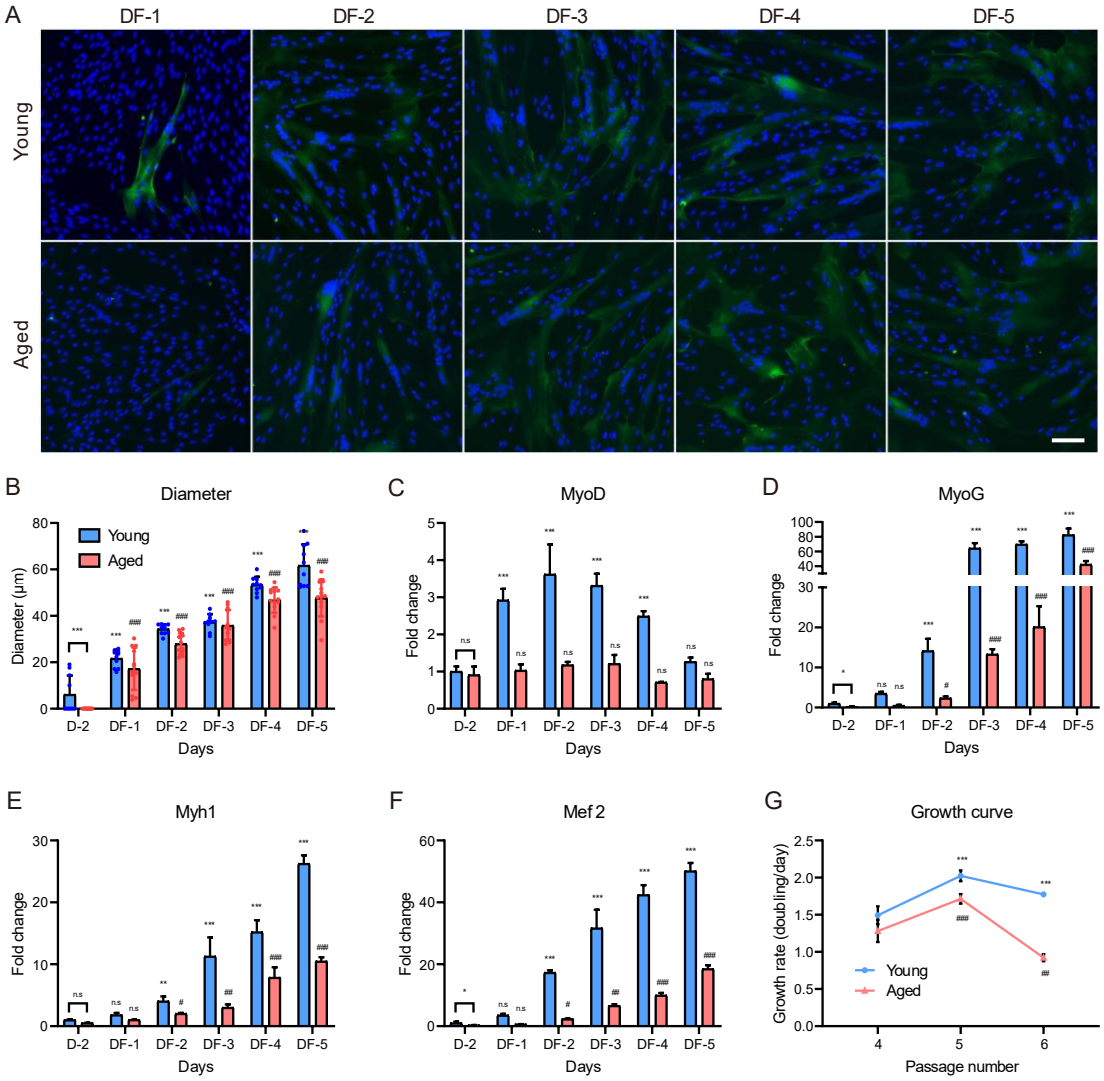

Fig. S6. Myotube formation and expression of genes related to differentiation. (A and B) Representative images (A) and quantification (B) of myotubes stained with Myh1 and nuclei, respectively. DF indicates differentiation date. Scale bar, 100 μm. (C-F) mRNA expression levels of MyoD (C), MyoG (D), Myh1 (E), and Mef2 (F). (G) Growth curve of hYskMC and hAskMC. (* P<0.05; ** P<0.01; *** P<0.001; compared to young control, # P<0.05; ## P<0.01; ### P<0.001; compared to aged control).

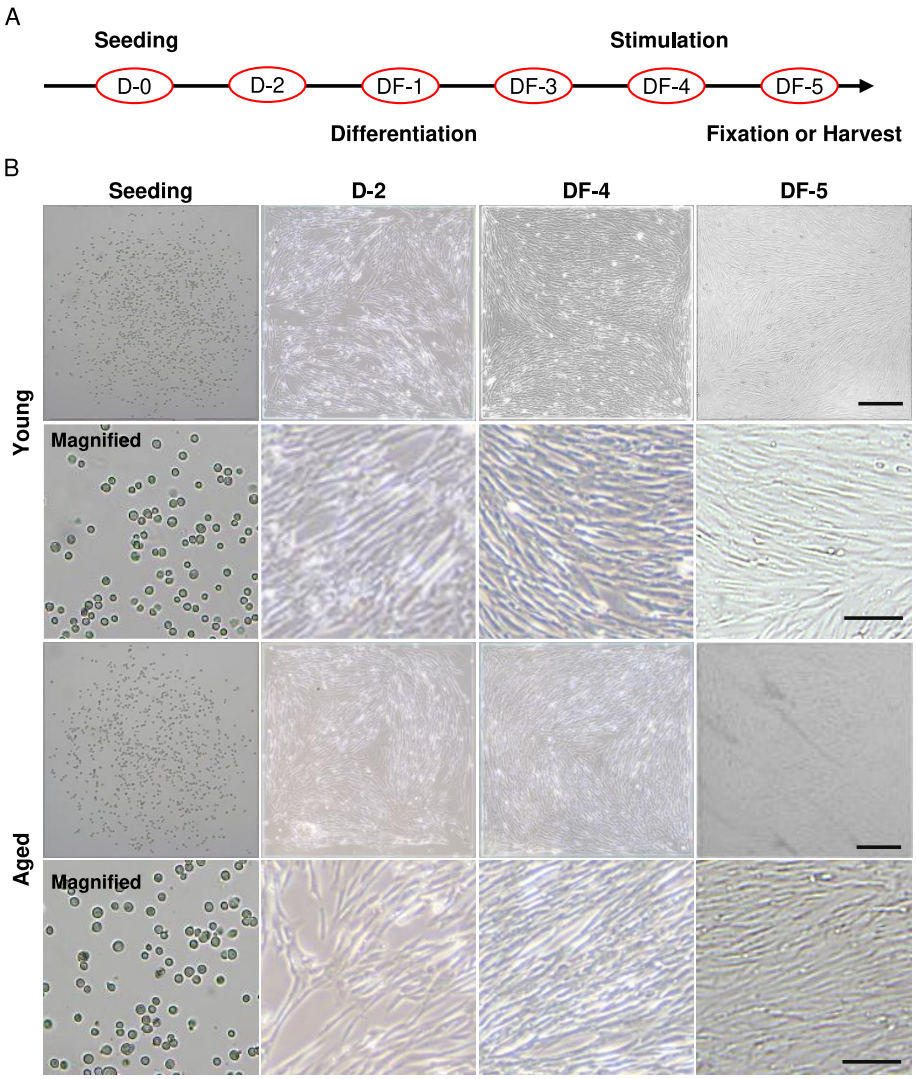

Fig. S7. In vitro experimental process. (A) Timeline of cell culture and ES. hYskMC and hAskMC were seeded onto the HiTESS substrate (D-0). After two days of cell proliferation, the medium was replaced with a differentiation medium. After four days of differentiation (DF), ES was performed. The cells were harvested and analyzed 24 h after ES application. (B) Images of the young and aged skeletal muscle cells upon seeding, Day-2, DF-4, and DF-5. Scale bar, 500 μm for the first row, and 100 μm for the second row, respectively.

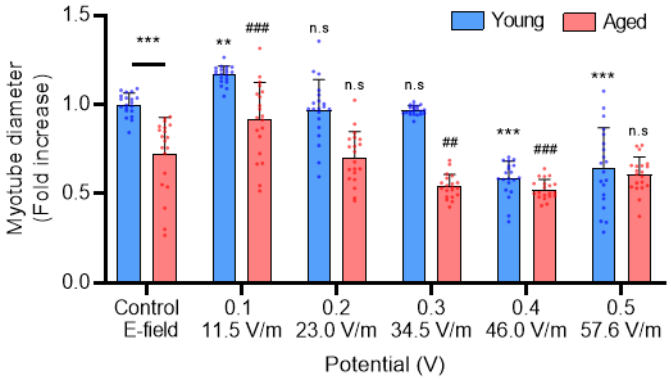

Fig. S8. Myotube diameters changed according to E-fields (voltage) in hYskMC and hAskMC. As 11.5 V/m showed the maximal increase in myotube thickness in both hYskMC and hAskMC, the optimal E-field was determined.

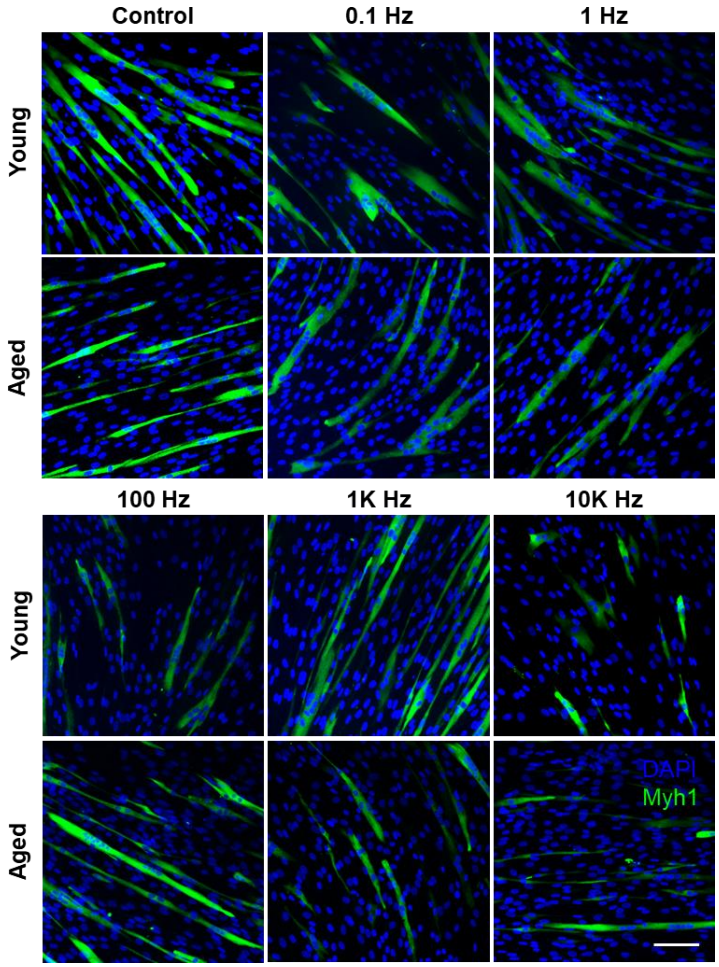

Fig. S9. Effect of frequency-dependent ES on myotube differentiation. While there was no significant change at 0.1 and 1 Hz, muscle atrophy was shown at 1k and 10k Hz ES conditions. Green, Myh1; blue, nuclei. Scale bar, 100 μm.

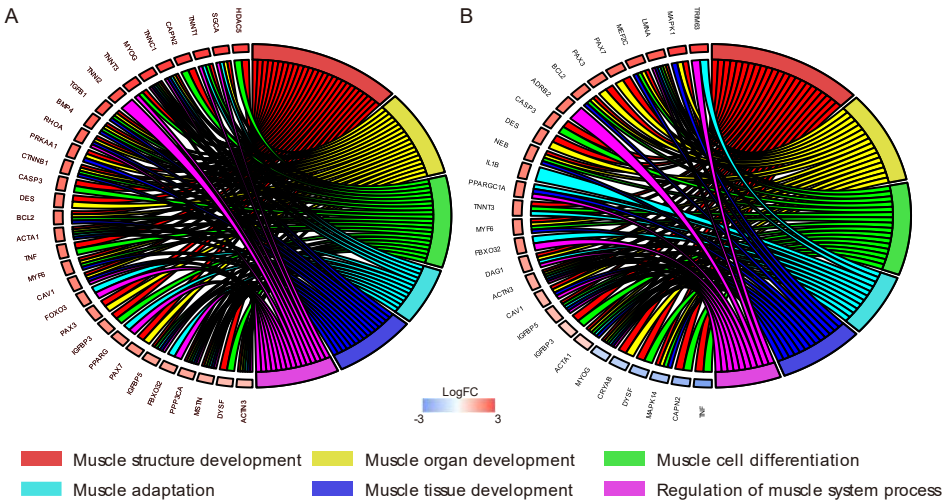

Fig. 10. Specific ES conditions induce increases in hypertrophy-related gene expression. (A and B) Gene ontology analysis results for hYskMC relative to hAskMC (A) and for aged 500 Hz relative to hAskMC control (B).

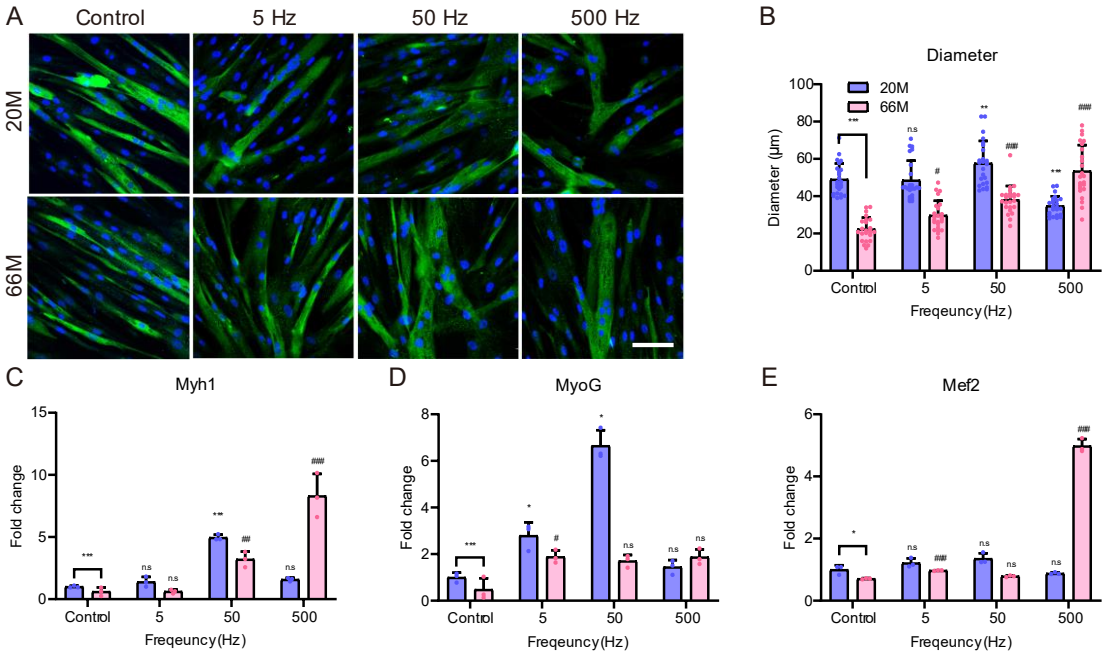

Fig. S11. Effects of ES on myotube formation in skMC from 20-year-old (20M) and 66-year-old (66M) males. (A and B) Representative images (A) and quantification (B) of myotubes stained with Myh1 (Green) and nuclei (Blue), respectively. Scale bar, 100 μm. (C-E) mRNA expression levels of Myh1 (C), MyoG (D), and Mef2 (E). (* P <0.05; ** P<0.01; *** P<0.001; compared to young control, # P<0.05; ## P<0.01; ### P<0.001; compared to aged control).

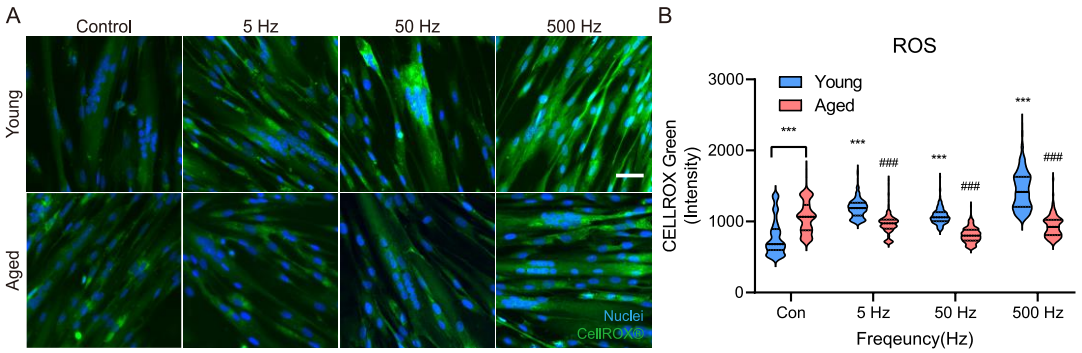

Fig. S12. Changes in intracellular ROS following ES conditions. (A and B) Representative images (A) and quantification (B) of myotubes stained with CellROX and nuclei, respectively. The intracellular ROS level of hAskMC tended to decrease by ES, and hYskMC increased slightly at 5 and 50 Hz and increased significantly at 500 Hz. Scale bar, 50 μm. (* P<0.05; ** P<0.01; *** P<0.001; compared to young control, # P<0.05; ## P<0.01; ### P<0.001; compared to aged control).

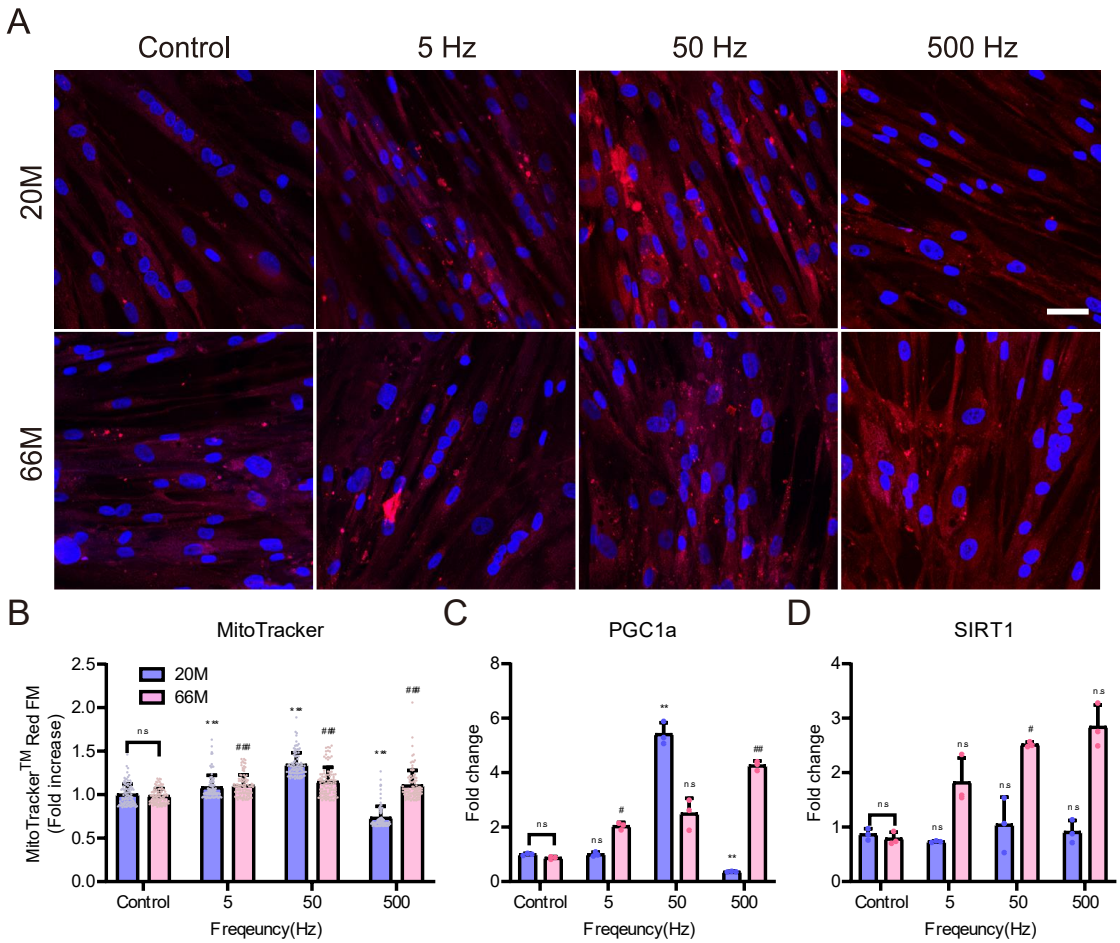

Fig. S13. Effects of ES on myotube metabolic functions in skMC from 20-year-old (20M) and 66-year-old (66M) males. (A and B) Representative images (A) and quantification (B) of MitoTracker™ Red FM staining of skMC. Scale bar, 100 μm. (C and D) mRNA expression level of PGC1a (C) and SIRT1 (D). (* P <0.05; ** P<0.01; *** P<0.001; compared to young control, # P<0.05; ## P<0.01; ### P<0.001; compared to aged control).

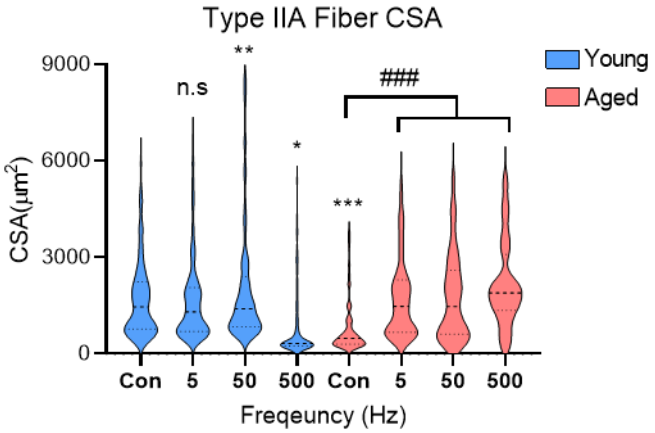

Fig. S14. Cross-sectioned area (CSA) of the Type IIA fiber in TA muscles of young and aged mice. The specific ES condition (500 Hz) significantly induced an increment of Type IIA muscle fiber CSA in aged mice (* P<0.05; ** P<0.01; *** P<0.001; compared to young control, # P<0.05; ## P<0.01; ### P<0.001; compared to aged control).

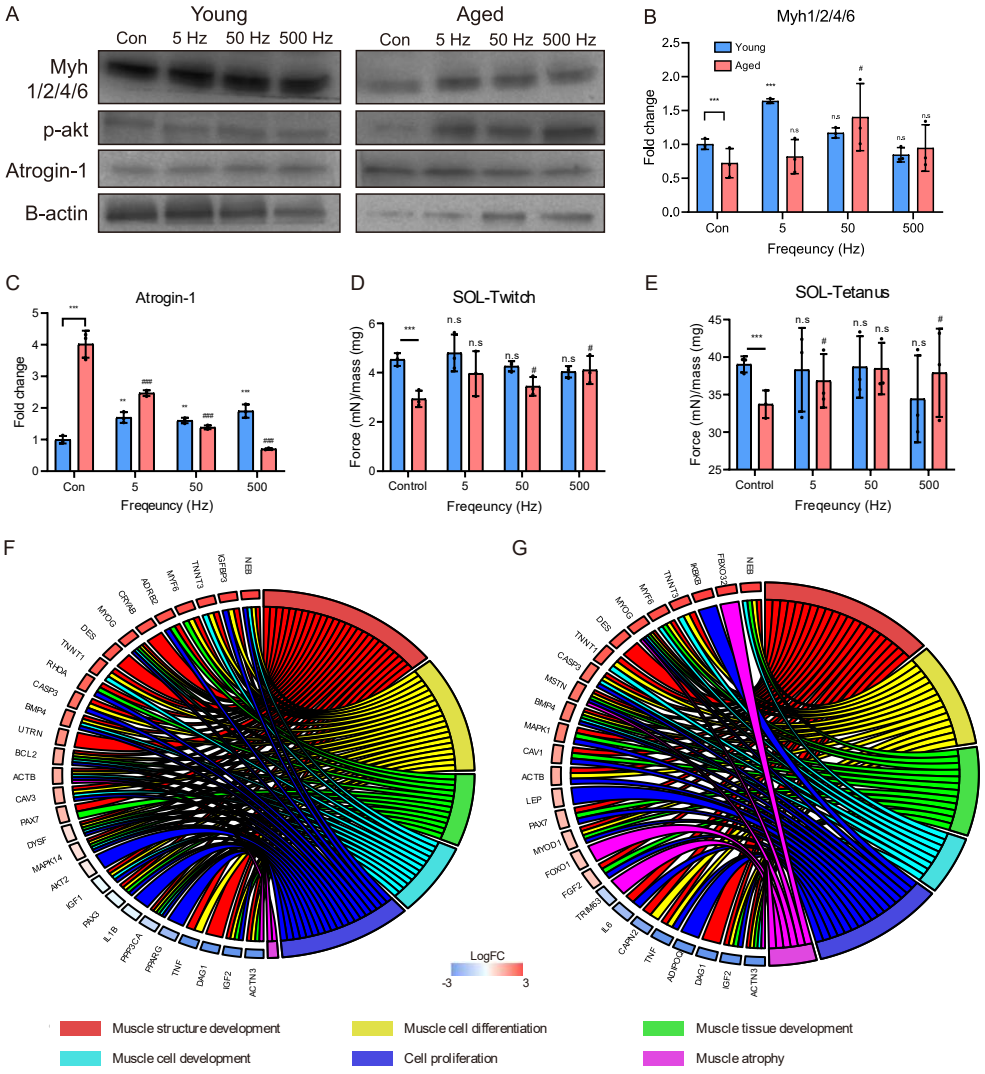

Fig. S15. Validation of the silver electroceutical in young and aged mice. (A-C) Results of protein expression related to hypertrophy and atrophy representative image (A) and quantification result of Myosin (Myh1/2/4/6) (B) and Atrogin-1 (C). (D and E) Normalized Isometric twitch (D) and tetanus contraction (E) force measurement of soleus muscles depending on ES conditions in young and aged mice. (F and G) Ontology analysis to investigate the molecular recovery of young skeletal muscle tissues with ES. Gene ontology analysis results of young 50 Hz (F) and young 500 Hz (G) compared to young control mice. (* P<0.05; ** P<0.01; *** P<0.001; compared to young control, # P<0.05; ## P<0.01; ### P<0.001; compared to aged control).

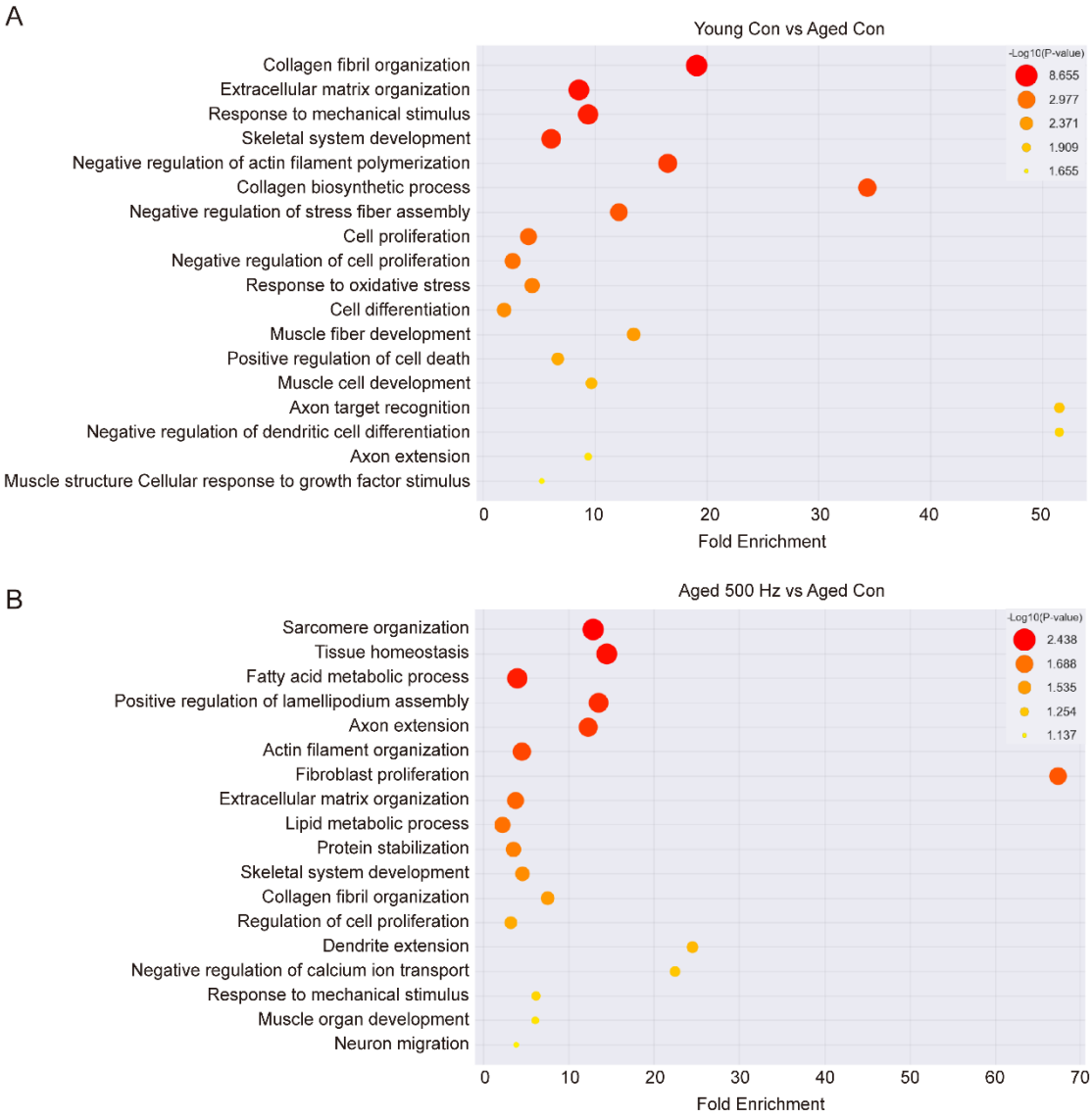

Fig. S16. Ontology analysis to investigate the molecular recovery of aged skeletal muscle tissues with ES. (A and B) Gene ontology analysis results of young control (A) and aged 500 Hz (B) compared to aged control. The ES condition induced young phenotypic ontological changes in aged mice.

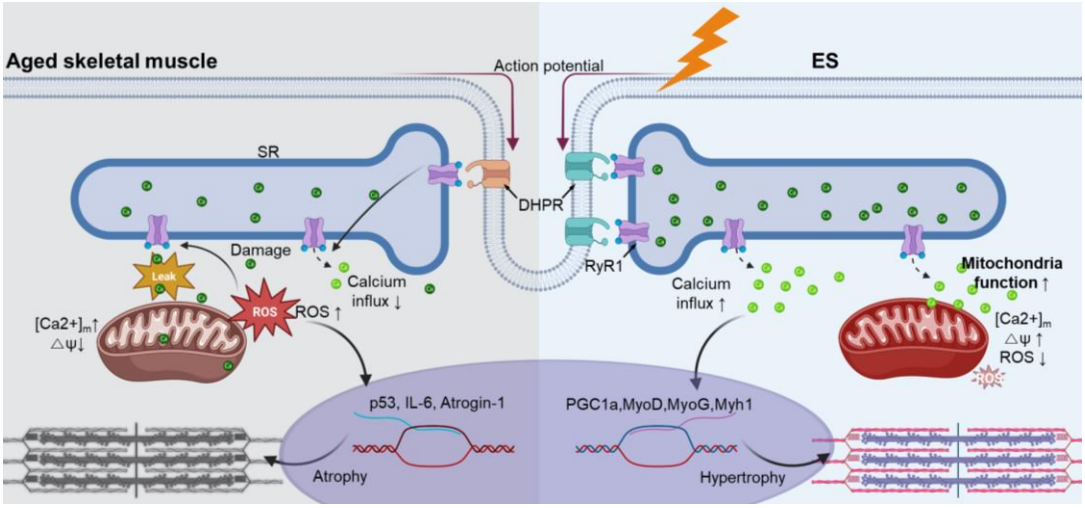

Fig. S17. Schematic of ES-mediated improvements in aged skeletal muscle. In aged skeletal muscle, there is a disruption in calcium homeostasis, since (i) the expression of DHPR and RyR1 decreases, resulting in reduced stimuli-responsive calcium influx, and (ii) there is chronic calcium leak from the SR. This causes mitochondrial dysfunction, elevating intracellular ROS level. The elevated ROS promotes the expression of inflammatory genes, leading to atrophy. However, after ES, there is a restoration of calcium homeostasis, which improves mitochondrial function, reduces intracellular ROS level, and induces the expression of genes related to hypertrophy.

Table S1. Specification of the HiTESS pulse generator

	Specification
Potential range	-10~10 (V)
Pulse width	0.0025 ms ~ 160 s
Frequency range	0.01 ~ 50k Hz
Channel	16 channels

Table S2. Antibody list for the immunocytochemistry

Gene	Company	Cat	Dilution
MF20 (MYH)	DSHB	MF20-S	1:200
SC-71 (Type IIa)	DSHB	SC-71-S	1:200
PAX7	DSHB	PAX7-S	1:200
Anti-Laminin Antibody	Sigma	L9393-.2ML	1:200
MYH1/2/4/6	SantaCruz	SC-32732	1:1000
Atrogin-1	ECM Biosciences	AP2041	1:1000
Goat anti-Mouse IgG1 Cross-Adsorbed Secondary Antibody, Alexa Fluor 488	Invitrogen	A21121	1:1000
Goat anti-Mouse IgG (H+L), Superclonal™ Recombinant Secondary Antibody, Alexa Fluor 488	Invitrogen	A28175	1:1000
Alexa Fluor® 594 AffiniPure Donkey Anti-Rabbit IgG (H+L)	Jackson Immuno Research Inc.	711-585-152	1:1000
Goat anti-Rabbit IgG (H+L) Secondary Antibody, HRP	Invitrogen	65-6120	1:1000
Goat anti-Mouse IgG (H+L) Secondary Antibody, HRP	Invitrogen	62-6520	1:1000

Table S3. Primer sequences for conventional RT-PCR on human-derived primary skeletal muscle cells

Gene	Forward primer sequence (5'-3')	Reverse primer sequence (5'-3')
Myh1	AGCTGATGACCAACTTGCGC	CCCTGGAGACTTTGTCTCATTAGG
MyoD	GCCACAACGGACGACTTCTA	AGTGCTCTTCGGGTTTCAGG
Mrf4	AATCTTGAGGGTGCGGATTTC	GGCTGACGAATCAATACTTGC
PGC1a	CACGGACAGAACTGAGGGAC	TTCGTTTGACCTGCGCAAAG
MEF2	GCACCAACAAGCTGTTCCAG	TGTCTGAGTTTGTCCGGCTC
Bcl-2	CTTTGAGTTCGGTGGGGTCA	GAAATCAAACAGAGGCCGCA
Akt	GGACAAGGACGGGCACATTA	CGACCGCACATCATCTCGTA
P16	CTTCGGCTGACTGGCTGG	AGACCCTCTACCCACCTGGA
P53	TCCCCAGCCCTTTTGTTGA	TTAGAACCAAATGTGGCCGTG
TNFa	GCCAGAGGGCTGATTAGAGA	CAGCCTCTTCTCCTTCCTGAT
MuRF1	AAGCCAGTGGTCATCTTGCC	CCAGTAGGGATTTGCAGCCT
B-actin	AGGCACCAGGGCGTGAT	GCCCACATAGGAATCCTTCTGAC
Myogenesis and myopathy array kit	AccuTarget™ qPCR Screening Kit (Bioneer SM-0148)	
Myogenesis array kit	AccuTarget™ qPCR Screening Kit (Bioneer SH-00148)	

Table S4. Biomaterial properties for three tissues used in the multiphysics simulation

Tissue	Density (kg/m^3)	Dielectric const.	Electric conductivity (S/m)
Bone	1908	2.70E+03	2.02E-02
Skeletal muscle	1090	4.35E+05	4.05E-1
Skin	1109	1.14E+03	1.22E-03

SI Reference

1. A. Moreno-Garcia, A. Kun, O. Calero, M. Medina, M. Calero, An Overview of the Role of Lipofuscin in Age-Related Neurodegeneration. *Front Neurosci* **12**, 464 (2018).
2. Q. Lang *et al.*, AC Electrothermal Circulatory Pumping Chip for Cell Culture. *ACS Appl Mater Interfaces* **7**, 26792-26801 (2015).
3. H. Y. Shin *et al.*, Cell Seeding Technology for Microarray-Based Quantitative Human Primary Skeletal Muscle Cell Analysis. *Anal Chem* **91**, 14214-14219 (2019).
4. E. Picht, A. V. Zima, L. A. Blatter, D. M. Bers, SparkMaster: automated calcium spark analysis with ImageJ. *Am J Physiol Cell Physiol* **293**, 1073-1081 (2007).
5. Hasgall PA *et al.*, "IT'IS Database for thermal and electromagnetic parameters of biological tissues," Version 4.1, Feb 22, 2022, itis.swiss/database